Check for updates

Proceedings of the ASME 2026 45th International Conference on Ocean, Offshore and Arctic Engineering
OMAE2026
June 7-12, 2026, Tokyo, Japan

OMAE2026-182297

Downloaded from asmedigitalcollection.asme.org/OMAE/proceedings-pdf/OMAE2026/89503/V003T03A008/7643707/v003t03a008-omae2026-182297.pdf by Deutsches Zentrum für Luft- und Raumfahrt (DLR) user on 02 October 2026

INFLUENCE OF ARTIFICIAL SEAWATER CORROSION ON THE FATIGUE STRENGTH OF 40 MM THICK WELDED DETAILS FOR OFFSHORE WIND SUPPORT STRUCTURES

Sulaiman Shojai
German Aerospace Center (DLR), Institute of Maritime Technologies and Propulsion Systems, Geesthacht, Germany

Christian Woitzik
TU Hamburg - Institute for Ship Structural Design and Analysis, Hamburg, Germany

Moritz Braun
German Aerospace Center (DLR), Institute of Maritime Technologies and Propulsion Systems, Geesthacht, Germany

Sören Ehlers
German Aerospace Center (DLR), Institute of Maritime Technologies and Propulsion Systems, Geesthacht, Germany

ABSTRACT

Offshore wind support structures are exposed to cyclic loading and harsh environmental conditions that can promote corrosion and potentially affect fatigue performance. This study investigates the influence of long-term artificial seawater corrosion on the fatigue strength of thick welded steel details representative of offshore applications. Butt-welded and fillet-welded joints with plate thickness of 40 mm were exposed to artificial seawater for 12 months and subsequently tested under four-point bending fatigue loading. Changes in weld geometry induced by corrosion were quantified using optical 3D surface scans. The results show that artificial seawater does not reduce the characteristic fatigue strength of the investigated joints. While butt welds exhibit comparable fatigue performance before and after corrosion, fillet welds show an increase in fatigue strength due to corrosion-induced smoothing of the weld toe geometry. These findings indicate that corrosion-induced surface modifications should be considered in fatigue assessment and lifetime extension strategies for offshore wind support structures.

Keywords: Offshore wind support structures; fatigue strength; welded joints; artificial seawater corrosion; 3D surface scanning; weld geometry; lifetime extension

NOMENCLATURE

A_5	elongation at fracture [%]
K_t	elastic stress concentration (notch) factor [–]
m	slope of the S–N curve [–]
N	number of cycles to failure [–]
r	weld toe radius [mm]
t	component thickness [mm]
T_σ	scatter coefficient of fatigue strength [–]
$\Delta\sigma_n$	nominal stress range [N/mm²]
$\Delta\sigma_c$	characteristic fatigue strength at N = $2 \cdot 10^6$ cycles [N/mm²]

1. INTRODUCTION

Offshore support structures are exposed to cyclic loading and harsh environmental conditions, which can promote corrosion even in the presence of corrosion protection systems. Corrosion can result not only in material loss but also in material embrittlement, with its influence on fatigue performance strongly depending on whether it occurs above or below the waterline. Below the water surface, both material loss and embrittlement can develop due to hydrogen accumulation, whereas above the waterline and the splash zone hydrogen can dissipate into the atmosphere and corrosion primarily leads to material loss. Material loss causes a reduction in cross-sectional thickness and, more critically, local changes in surface geometry due to pitting, which can act as stress concentrators and interact with existing weld-induced notches, thereby significantly affecting fatigue strength.

Previous studies have investigated the influence of pitting corrosion on fatigue performance by introducing artificial pits or by exposing specimens to accelerated laboratory corrosion prior to fatigue testing [1–6]. Investigations on material retrieved from decommissioned structures have also been reported [7,8]; however, these studies predominantly focus on base material rather than welded joints and/or are often limited to thin specimens that are of limited relevance for offshore wind applications. In the context of lifetime extension strategies for offshore support structures, it is essential to investigate representative thick welded specimens under realistic seawater exposure conditions without accelerated corrosion, and to account for surface preparation processes such as clean-blasting, which are required prior to coating and must comply with the

Copyright © 2026 by ASME; reuse license CC-BY 4.0

DNV RP-0416 [9], which requires the surfaces to be clean-blasted by grit to Sa 2½ according to ISO 8501-1 [10] with a roughness 50-85 µm according to ISO 8503 [11]. To address this knowledge gap, the present study examines thick steel specimens with both butt- and fillet-welded joints, representative of maritime structures, after one year of exposure to artificial seawater. The fatigue performance of the corroded specimens is evaluated through fatigue testing and compared to uncorroded reference specimens, while optical measurements conducted before and after exposure are used to quantify weld geometry and corrosion-induced material loss.

2. MATERIALS AND EXPERIMENTS

2.1 Specimens preparation and geometry

Within the scope of this investigation, welded specimens with a thickness of 40 mm manufactured from the low-alloy structural steel EN 10225 S355G10+M, comparable to ASTM A131 EH36, were analyzed. The mechanical properties of the material are summarized in **TABLE 1**, while the specimen geometries used in the experimental program are illustrated in **FIGURE 1**.

TABLE 1: Material properties S355G10+M

Chemical composition [%]								
C	Si	Mn	P	S	N	Al	Cu	Cr
0.06	0.27	1.37	0.012	0.001	0.005	0.036	0.02	0.03
Mechanical properties:								
Yield stress $R_{p0.2}$ [N/mm²]			Ultimate strength R_m [N/mm²]			Elongation A5 [%]		
421			493			35		

Two welded joint configurations were considered: double V-groove butt joints and fillet-welded joints.
The butt-welded specimens were produced using the submerged arc welding (SAW) process, corresponding to process 121 in accordance with ISO 4063, in the flat welding position (PA). Welding was performed with a solid wire filler material S3Si. Prior to welding, the joint preparation involved mechanical grinding, and the weld metal was deposited in multiple passes to achieve full penetration while maintaining controlled heat input. The fillet-welded specimens comprised non-load-carrying transverse stiffeners welded onto a continuous base plate. These fillet welds were executed with a throat thickness of 12 mm and consisted of two individual weld layers. Welding was carried out using the metal active gas (MAG) process with a metal-cored wire, corresponding to process 138 according to ISO 4063. The filler material was classified as EN ISO 17632-A T46 6 M M 1 H5 and was used in conjunction with an M21 shielding gas. No preheating or post-weld heat treatment was applied; instead, the joint area was mechanically ground and cleaned prior to welding to ensure reproducible welding conditions.

For both joint types, the allowable limits for weld imperfections were specified in accordance with evaluation group B as defined in ISO 5817[12].
Following welding, the specimens were sectioned into strips with a width of 70 mm from a steel plate measuring 1000 mm in length and 500 mm in width using water jet cutting. Subsequently, the specimens were subjected to clean blasting in compliance with the requirements of DNV RP-0416 [9], which are applicable to offshore support structures, to clean and roughen the surface in preparation for the later application of corrosion protection. Grit was used as the blasting medium, and surface cleanliness levels ranging from Sa 2½ to Sa 3 in accordance with ISO 8501-1 were achieved.
After clean blasting, corrosion protection was applied only to the end regions of the specimens in order to limit the formation of corrosion products during the corrosion exposure. The weld regions themselves were intentionally left unprotected. The edges were chamfered to prevent crack initiation at these locations. In addition, the support surfaces required for four-point bending fatigue tests were face-milled to ensure flatness and parallelism, thereby enabling uniform load introduction despite angular distortions caused by welding. This machining step was necessary for both the uncorroded reference specimens and the specimens exposed to artificial seawater, as welding-induced distortion was present in all cases. The corresponding machined areas are also indicated in **FIGURE 1**.

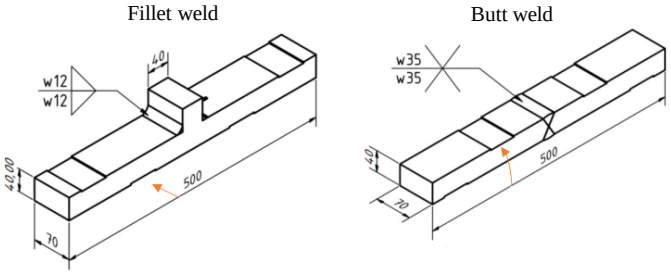


FIGURE 1: Specimens geometries

TABLE 2: Fatigue test program

Specimen geometry: / Condition:	Butt weld	Fillet welds
Clean blasted - uncorroded	15	15
Clean blasted – corroded 12-months in artificial saltwater	15	15

2.2 Artificial seawater setup

After specimen preparation, the samples were immersed in a water basin filled with artificial seawater. The artificial seawater was prepared in accordance with ASTM D1141–98 [13] , using the formulation without additional heavy metals [14]. The corresponding chemical composition is summarized in **TABLE 3**. At the beginning of the exposure period, the pH value of the

Downloaded from asmedigitalcollection.asme.org/OMAE/proceedings-pdf/OMAE2026/89503/V003T03A008/7643707/v003t03a008-omae2026-182297.pdf by Deutsches Zentrum für Luft- und Raumfahrt (DLR) user on 02 October 2026

Copyright © 2026 by ASME; reuse license CC-BY 4.0

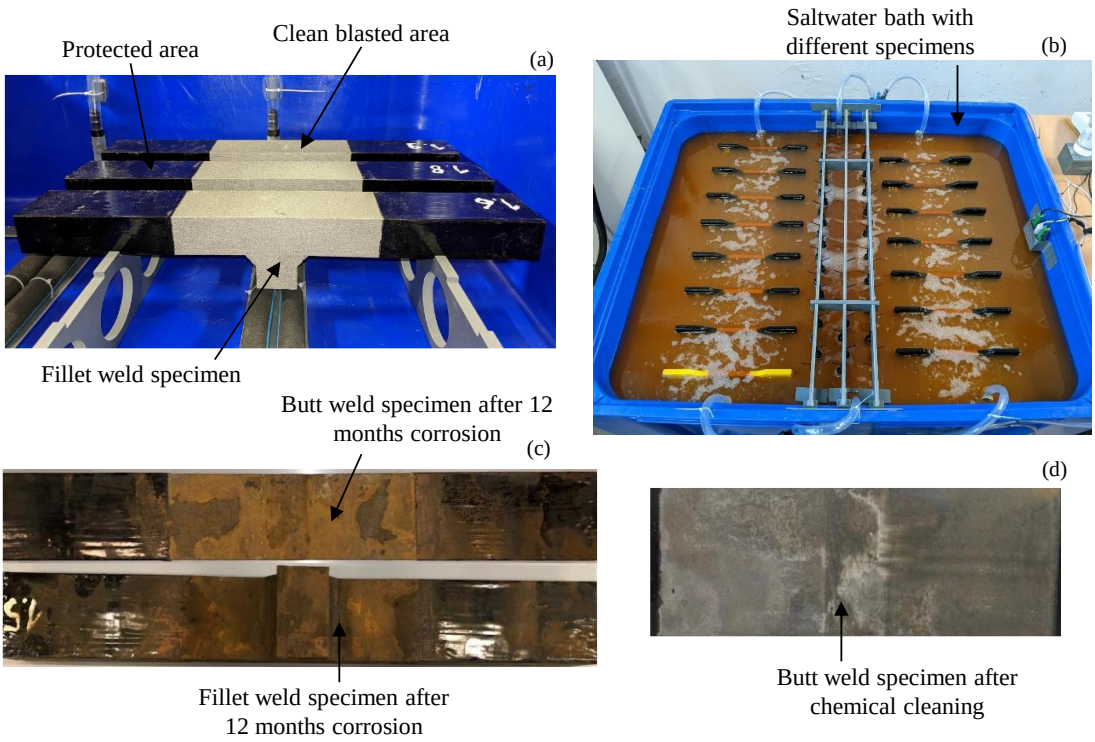


FIGURE 2: Artificial seawater bath setup: (a) fillet-welded joint specimens immersed in the artificial seawater bath, (b) artificial seawater bath during operation, (c) specimens after removal from the seawater bath, and (d) specimen surface condition after derusting.

water was adjusted to 8.2 using sodium hydroxide. Throughout the entire duration of the experiment, the water temperature, electrical conductivity, and pH value were continuously monitored and recorded. No relevant changes in these parameters were observed over the 12-month exposure period; the pH value was adjusted when necessary to maintain stable test conditions.

TABLE 3: Composition of the artificial seawater

Chemical composition [g/l]									
NaCl	MgCl2	Na2SO4	CaCl2	KCl	NaHCO3	KBr	H3BO3	SrCl2	NaF
24.53	5.2	4.09	1.16	0.695	0.201	0.0101	0.027	0.025	0.003

The specimens were stored in a pallet box with internal dimensions of 1115 mm × 915 mm and a height of 600 mm, as illustrated in **FIGURE 2** (a) and (b). To avoid interference with the corrosion process, spacers made of PVC were used. In addition, the surface area of the specimens exposed to seawater was deliberately limited by coating the specimen ends, as previously described and shown in **FIGURE 2** (a). This approach not only reduced the overall amount of corrosion products but also prevented excessive rust formation from adversely affecting the corrosion process.

Approximately 500 L of artificial seawater were required to completely submerge all specimens in the container. To achieve more realistic environmental conditions, the water was circulated by air injection. Two of the six inlet hoses are visible beneath the specimens in **FIGURE 2** (a). A maximum flow rate of 900 L/h resulted in a clearly observable water movement and additionally promoted oxygen enrichment of the artificial seawater. The final experimental setup is shown in **FIGURE 2** (b). To minimize water loss due to evaporation, the basin was covered during operation and the water level was replenished as required.

The corroded specimens were exposed to the artificial seawater environment for a period of 12 months. After removal from the basin, loosely adhering corrosion products and surface contaminants were manually removed, resulting in a surface condition as shown in **FIGURE 2** (c). Subsequently, the specimens were chemically cleaned to remove the remaining corrosion products. For this purpose, a hydrochloric acid solution with antimony trioxide was applied in accordance with DIN EN ISO 8407, solution C.3.2 [15]. This cleaning step was particularly necessary for the subsequent surface scanning of the specimens. A cleaning duration of approximately 20 minutes proved to be sufficient, and in combination with gentle mechanical brushing, all residual corrosion products could be removed. The surface condition after derusting is shown in **FIGURE 2** (d).

2.3 3D scans

Three-dimensional surface measurements were performed using an optical ATOS Core 5M 3D scanner (GOM) with a spatial resolution of 0.12 mm. The scanner was positioned at a distance of 500 mm from the specimen, which was mounted on a rotatable stage to enable image acquisition from multiple viewing angles.

Copyright © 2026 by ASME; reuse license CC-BY 4.0

Downloaded from asmedigitalcollection.asme.org/OMAE/proceedings-pdf/OMAE2026/89503/V003T03A008/7643707/v003t03a008-omae2026-182297.pdf by Deutsches Zentrum für Luft- und Raumfahrt (DLR) user on 02 October 2026

The acquired scans were automatically aligned and merged using GOM Suite software, provided that a sufficient number of reference points was available; therefore, reference markers were attached to the rotatable plate. Typically, four individual scans were sufficient to capture each side of a specimen. To combine the scans of both sides into a single model, additional reference markers were applied to the lateral surfaces of the specimens, allowing complete scanning with a total of eight reference points. All specimens listed in **TABLE 2** were scanned following this procedure, while corroded specimens were scanned both before and after corrosion exposure. The final output of the scanning process was an STL file, representing a surface generated from a triangulated point cloud, as illustrated in **FIGURE 3**.

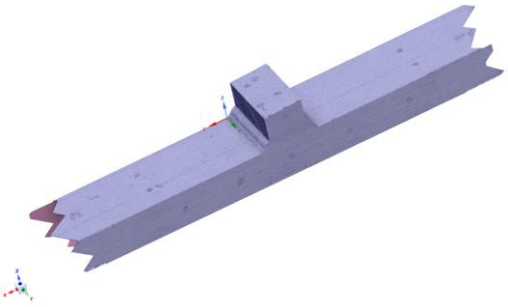


FIGURE 3: Example of a fillet-welded specimen captured by 3D scanning and exported in STL format.

The generated STL files were used for the quantitative evaluation of weld geometry parameters as well as for digital surface comparisons before and after corrosion exposure. The surface comparison was performed using the GOM Suite software by importing both scans into a single project and manually pre-aligning them. Following this initial positioning, the datasets were superimposed using a best-fit alignment based on a least-squares approximation.

2.4 Weld parameter characterization

Weld geometry plays a crucial role in fatigue assessment, as it directly governs local stress concentrations, which are a key driving parameter for fatigue strength. The weld geometry of each specimen is characterized by the weld toe radius r and the flank angle θ, in accordance with ISO 5817 [12] (see **FIGURE 4** (a)). Based on these geometric parameters, the elastic stress concentration factor (notch factor K_t) can be determined using various analytical formulations for welded joints, as summarized by Radaj et al. [16], including, for example the following equation proposed by Anthes et al. [17]:

$$K_t = 1 + 0.728(\sin(180° - \theta))^{0.932}\left(\frac{t}{r}\right)^{0.382} \qquad (1)$$

In this formulation the notch factor K_t depends on the weld toe radius r, the flank angle θ and the component thickness t and increases with larger flank angles, larger notch radii, and decreasing thickness. To quantify the effect of corrosion on fatigue performance, it is therefore essential to analyze the weld geometry parameters and their changes induced by corrosion. In recent years, several fully digital approaches for evaluating the real geometry of welded components have been developed, for instance by Renken et al.[18], Schubnell et al. [19] and Dänekas et al. [20] . In the present study, the geometric parameters were evaluated using a MATLAB-based tool specifically developed for corroded specimens and relying on a least-squares methodology. The analysis is based on 3D scan data obtained with the ATOS system, which are processed as point clouds in ASCII format. The surface geometry is evaluated along the longitudinal direction using all recorded data points, resulting in a series of longitudinal cross sections.

For each cross section, the first derivatives of the height coordinates are calculated to identify the point of maximum slope within the weld seam (point A) and the weld toe (point B). These points are subsequently used to determine the balance lines of the surface—one representing the base material and one representing the weld seam (see **FIGURE 4** (b)). The flank angle is defined as the angle between these two balance lines. Their intersection serves as the reference point for fitting a circular arc to the weld toe region, where the notch radius is determined by minimizing the sum of squared deviations between the fitted circle and the measured surface data. For fillet-welded specimens, the geometric parameters were evaluated for two welds (left and right), whereas for butt-welded specimens the analysis was conducted at four locations (two on the upper and two on the lower side). All geometric parameters were determined for both the corroded and uncorroded conditions.

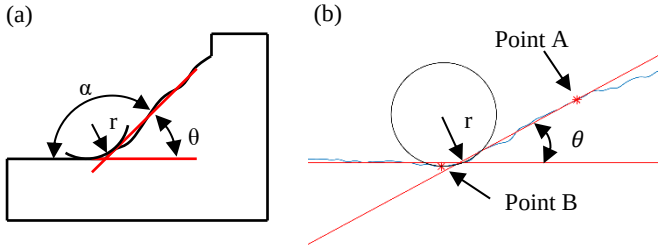


FIGURE 4: (a) Geometrical weld parameters according ISO 5817 [12] and (b) Implementation in the MATLAB tool.

2.5 Fatigue tests

Fatigue strength tests were performed using a mechanical resonance pulsator with a maximum load capacity of 200 kN in both tension and compression. Due to the relatively large specimen thickness of 40 mm, the experiments were conducted under bending loading using a four-point bending fixture at the stress ratio of R = 0.3. The experimental setup is illustrated in **FIGURE 5** (a).

The specimen was mounted transversely to the loading direction of the pulsator and supported between two bearing beams. On the support side, the distance between the bearing points was 450 mm, while on the load introduction side, the spacing between the loading points was 200 mm. This configuration resulted in a constant bending stress region in the central part of the specimen,

Downloaded from asmedigitalcollection.asme.org/OMAE/proceedings-pdf/OMAE2026/89503/V003T03A008/7643707/v003t03a008-omae2026-182297.pdf by Deutsches Zentrum für Luft- und Raumfahrt (DLR) user on 02 October 2026

Copyright © 2026 by ASME; reuse license CC-BY 4.0

with the maximum bending stress occurring at the specimen surface and thus in the vicinity of the weld.

The specimen installed in the test rig is also shown in **FIGURE 5** (a). Owing to the operating principle of the resonance pulsator and the stiffness of the four-point bending fixture in combination with the specimen, a testing frequency of approximately 32 Hz was achieved, with slight variations depending on the applied load level. Abrupt or gradual changes in the test frequency may indicate crack initiation or propagation, as cracking alters the stiffness of the overall system. For the specimen configurations investigated in this study, testing was typically continued until clearly visible failure occurred, as shown in **FIGURE 5** (b) and (c).

Using this setup, a maximum bending stress of $\sigma_{b,max}$=670 N/mm² could be achieved. During the experimental program, the applied stress range varied between 200 N/mm² and 500 N/mm².

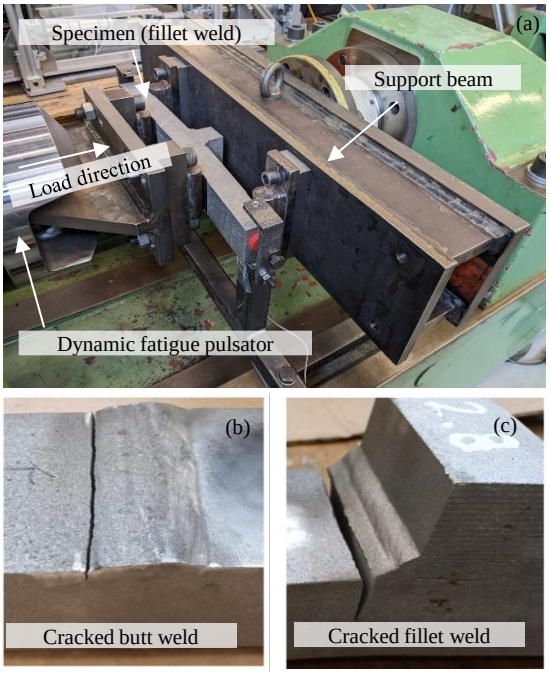


FIGURE 5: Specimen installed in the four-point bending fatigue test setup.

3. RESULTS AND DISCUSSION

3.1 Results 3D scans

The 3D scans were used to compare the surface condition of the specimens before and after corrosion exposure. **FIGURE 6** (a) shows the corrosion-induced material loss over the entire specimen surface for a butt-welded specimen as an example. For the butt-welded specimens, it can be observed that predominantly uniform corrosion occurred on both the upper and lower surfaces, with no pronounced formation of pitting corrosion. In addition, the material loss is mainly located in the base plate region. In the fatigue-relevant area at the weld toe, only minor and sporadic material loss is detectable.

A similar behavior can be observed for the fillet-welded specimens in **FIGURE 6** (b). However, in this case the material loss in the weld toe region appears more uniform and less sporadic compared to the butt-welded specimens.

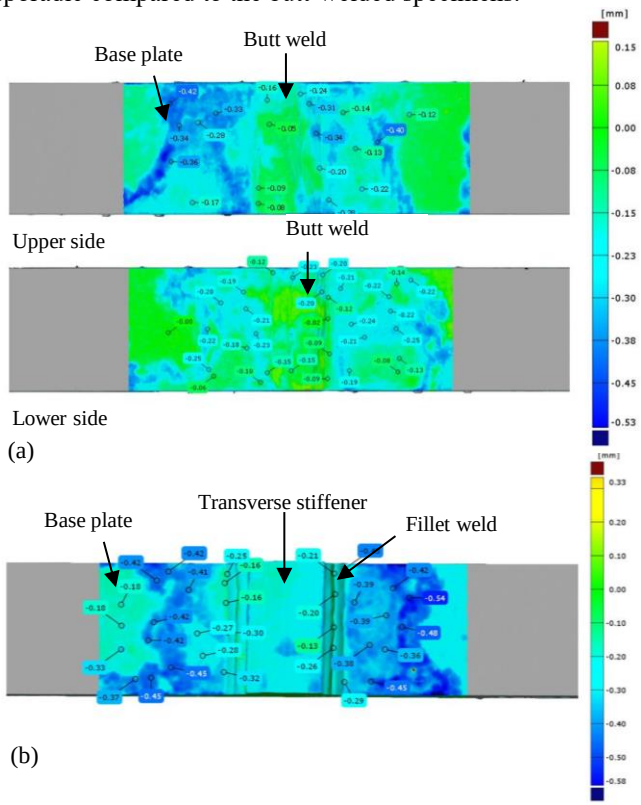


FIGURE 6: Results of the surface comparison before and after corrosion.

3.2 Results of weld parameter analysis

The results of the weld geometry evaluation for all tested specimens are shown in **FIGURE 7** . The values presented for each specimen represent the mean values of all evaluated cross sections. From **FIGURE 7** (a) it can be seen that the flank angles of the fillet-welded specimens are, as expected, larger than those of the butt-welded specimens. Correspondingly, the weld toe radii of the fillet welds are smaller than those of the butt welds, as shown in **FIGURE 7** (b).

For the fillet welds, corrosion leads to a reduction of the flank angle, while the weld toe radius remains nearly unchanged on average across all specimens. A smaller flank angle results, according to the formulation by Anthes et al. (Equation (1)), in a reduced notch stress, meaning that the notch becomes less severe.

In contrast, for the butt welds, the evaluated mean flank angles show either a slight increase or no relevant change after corrosion for most specimens. Since the values shown in **FIGURE 7** represent mean values of all evaluated cross sections, these small differences should be interpreted with caution and not overestimated as a systematic effect of corrosion.

Downloaded from asmedigitalcollection.asme.org/OMAE/proceedings-pdf/OMAE2026/89503/V003T03A008/7643707/v003t03a008-omae2026-182297.pdf by Deutsches Zentrum für Luft- und Raumfahrt (DLR) user on 02 October 2026

Copyright © 2026 by ASME; reuse license CC-BY 4.0

At the same time, a pronounced reduction of the weld toe radius is detected for nearly all butt-welded specimens. According to Equation (1), the reduction in weld toe radius is therefore considered the more relevant geometrical change and leads to an increase in notch stress, i.e. to a sharper notch.

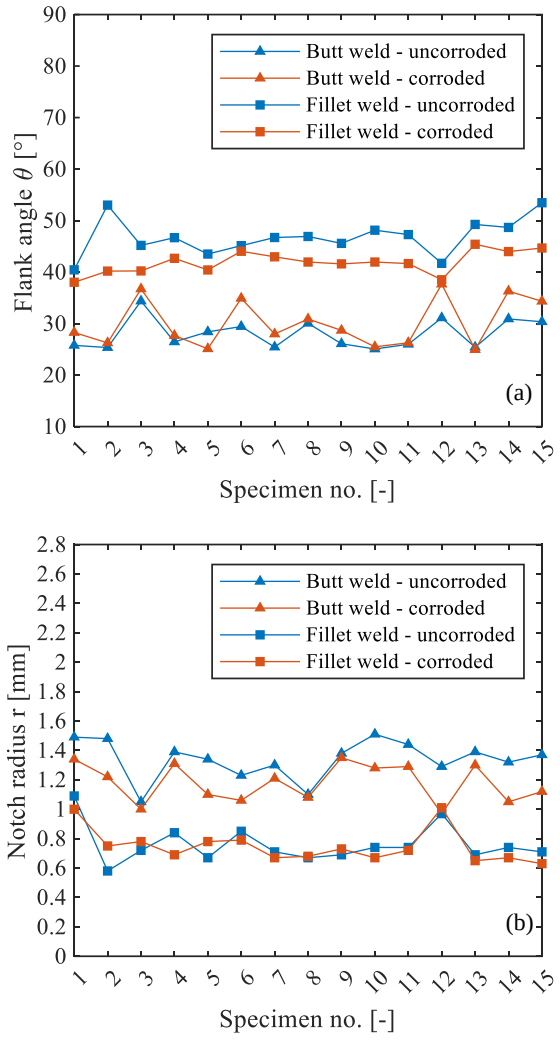


FIGURE 7: Evaluation of weld geometry parameters.

3.3 Results of fatigue tests

The fatigue test results were evaluated in accordance with Eurocode 3 [21] using linear regression based on the least-squares method in the direction of the number of cycles. Additional stress magnification factors resulting from specimen misalignments were not considered in this evaluation. Run-out specimens were excluded from the regression analysis and are therefore not shown in the corresponding diagrams; instead, these specimens were retested at an increased load level provided that no crack initiation was detected. For each test series, the associated S–N curves, defined as

$$N = 2 \cdot 10^6 \cdot \left(\frac{\Delta\sigma_c}{\Delta\sigma_n}\right)^m \quad (2)$$

were derived. In the equation, N represents the number of cycles to failure, $\Delta\sigma_n$ is the variable nominal stress range, m is the slope, and $\Delta\sigma_c$ is the characteristic stress range at $N = 2 \cdot 10^6$ cycles. Furthermore, the scatter coefficient T_σ was evaluated. This is defined as

$$T_\sigma = \frac{\Delta\sigma_{c,10\%}}{\Delta\sigma_{c,90\%}} \quad (3)$$

where $\Delta\sigma_{c,10\%}$ and $\Delta\sigma_{c,90\%}$ are the characteristic fatigue strengths derived from the S-N curve for 10 % and 90 % survival probability at $N = 2 \cdot 10^6$ cycles.

TABLE 4: Parameter of S-N curves

Geometry	Corrosion exposure	Slope m	Fatigue strength 50%-quantile $\Delta\sigma_c$ [N/mm²]	Fatigue strength 95%-quantile $\Delta\sigma_c$ [N/mm²]	Scatter T_σ
Butt welds	uncorroded	-5.9	254	207	1.37
	12M - S	-4.6	242	207	1.27
Fillet welds	uncorroded	-3.5	128	109	1.28
	12M - S	-3.6	129	115	1.18

In **FIGURE 8** the S–N curves for butt- and fillet-welded specimens in both the uncorroded and corroded conditions are presented. For the evaluation of the S–N curves, specimens tested up to 2 million load cycles were considered. For the butt welds in the uncorroded condition, a characteristic fatigue strength of $\Delta\sigma_c$ = 207 N/mm² is obtained with a slope of m = −5.9 and a scatter of T_σ = 1.37. After 12 months of corrosion exposure in artificial seawater, the butt-welded specimens show the same characteristic fatigue strength of $\Delta\sigma c$ = 207 N/mm², but with a reduced slope of m = −4.6 and a reduced scatter of T_σ = 1.27.

For the fillet welds, the uncorroded specimens exhibit a characteristic fatigue strength of $\Delta\sigma_c$ = 109 N/mm² with a scatter of T_σ = 1.28. After 12 months of corrosion exposure, the characteristic fatigue strength increases to $\Delta\sigma_c$ = 115 N/mm², while the scatter is reduced to T_σ = 1.18, with a similar slope of m = −3.6.

Finally, **FIGURE 9** compares the fatigue test results for all investigated conditions. For the butt welds, it can be observed that in the low-cycle fatigue regime the corroded specimens exhibit higher fatigue strength than the uncorroded specimens, while in the high-cycle fatigue regime the fatigue strength remains nearly unchanged. This behavior is attributed to a significant influence of corrosion on the slope of the S–N curves. For the fillet welds, the influence of corrosion is largely independent of the applied stress level. Corrosion leads to an overall improvement in fatigue strength across the entire investigated range. The slope remains nearly constant, while the

Downloaded from asmedigitalcollection.asme.org/OMAE/proceedings-pdf/OMAE2026/89503/V003T03A008/7643707/v003t03a008-omae2026-182297.pdf by Deutsches Zentrum für Luft- und Raumfahrt (DLR) user on 02 October 2026

Copyright © 2026 by ASME; reuse license CC-BY 4.0

S–N curve is shifted upward. For comparison, the corresponding Eurocode S–N curves for butt and fillet welds are also shown in

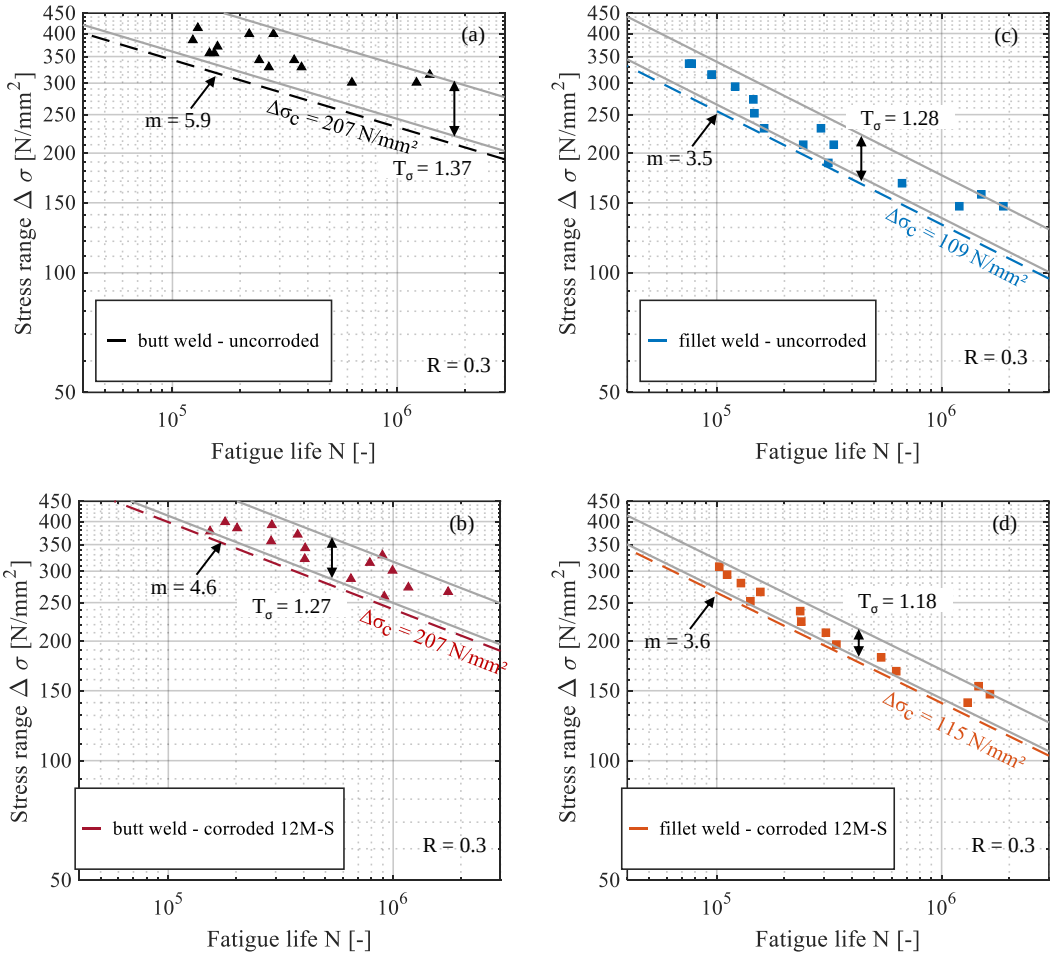


FIGURE 8: Fatigue test results: (a) uncorroded butt welds, (b) corroded butt welds, (c) uncorroded fillet welds, and (d) corroded fillet welds.

FIGURE 9 . The Eurocode FAT 90 curve for butt welds is exceeded by more than a factor of two, both before and after corrosion exposure. This is partly due to the bending loading applied in the present tests, but to a greater extent due to the clean-blasting of the specimens in accordance with offshore corrosion protection requirements. This beneficial effect is not reduced by the 12-month corrosion exposure.

A similar effect is observed for the fillet welds. Clean blasting results in an increased characteristic fatigue strength compared to the Eurocode FAT 80 curve. Although the increase is less pronounced than for the butt welds, the improvement is maintained or even enhanced after corrosion exposure.

3.4 Discussion

The fatigue tests demonstrate that 12 months of corrosion exposure in artificial seawater do not have a detrimental effect on the fatigue strength of 40 mm thick welded specimens. On the contrary, the fatigue strength of the fillet-welded specimens increases after corrosion exposure, while the fatigue strength of the butt-welded specimens remains at a comparable level. This increase builds upon an initial improvement caused by the clean-blasting process. Overall, the specimens exhibit fatigue strengths exceeding those specified in design standards even after corrosion exposure.

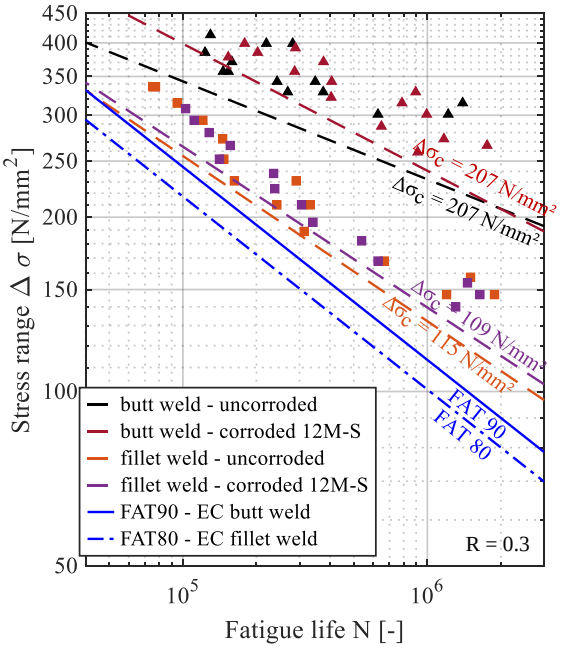
The observed increase in fatigue strength can be explained by the results of the 3D scans and weld geometry analyses. For the fillet welds, the 3D scans show a uniform material removal in the weld toe region, which is the critical location for fatigue crack initiation. This material loss reduces the flank angle, resulting in a less severe notch compared to the uncorroded condition. A milder notch delays fatigue crack initiation and therefore increases fatigue life.

For the butt welds, a slight increase in flank angle combined with a reduction in weld toe radius leads to a marginally sharper notch after corrosion. Despite this, the characteristic fatigue strength remains unchanged or is even higher in the low-cycle

Copyright © 2026 by ASME; reuse license CC-BY 4.0

Downloaded from asmedigitalcollection.asme.org/OMAE/proceedings-pdf/OMAE2026/89503/V003T03A008/7643707/v003t03a008-omae2026-182297.pdf by Deutsches Zentrum für Luft- und Raumfahrt (DLR) user on 02 October 2026

fatigue regime. An examination of the 50% quantile fatigue strength values in **TABLE 4** shows that uncorroded specimens exhibit higher values than corroded ones. However, the lower



characteristic fatigue strength of the uncorroded specimens is primarily caused by their higher scatter. When evaluating the 95% quantile fatigue strength, both uncorroded and corroded specimens show the same characteristic value of $\Delta\sigma_c$ = 207 N/mm², confirming the relationship between notch severity and fatigue strength also for butt-welded specimens.

FIGURE 9: Comparison of fatigue test results.

It should be noted that all fatigue tests were conducted in air. Offshore support structures include both submerged and above-water regions. Therefore, the conclusions drawn in this study are only valid for above-water regions. For submerged conditions, fatigue behavior differs due to the additional material embrittlement caused by hydrogen uptake, which accelerates crack initiation and propagation [22]. In addition, the results are limited to the investigated steel grade, specimen thickness, weld geometries, surface preparation condition and the specific 12-month laboratory exposure in artificial seawater.

A further noteworthy result is the comparatively shallow slope of the S–N curves for the butt-welded specimens in both the uncorroded and corroded conditions. This indicates that fatigue crack initiation contributed substantially to the overall fatigue life, whereas a slope closer to m = 3 would be expected for predominantly crack-propagation-controlled behavior. The slightly steeper slope of the corroded butt-welded specimens suggests earlier crack initiation in the corroded condition. However, based on the available test records, a reliable separation between crack initiation and crack propagation life was not possible. Although changes in the resonance frequency were monitored during testing, these records did not allow a robust identification of systematically earlier crack initiation in the corroded butt-welded specimens.

4. CONCLUSION

The objective of this study was to investigate the influence of corrosion on the fatigue strength of thick-walled welded joints representative of offshore support structures. Butt-welded and fillet-welded specimens made of structural steel were exposed to artificial seawater for 12 months. After exposure, the specimens were analyzed using 3D surface scans to quantify changes in weld geometry and subsequently tested under fatigue loading. The main findings can be summarized as follows:

- Corrosion leads to a reduction in fatigue strength scatter for both butt and fillet welds.
- For fillet welds, the characteristic 95% quantile fatigue strength increases from $\Delta\sigma_c$ = 109 N/mm² to $\Delta\sigma c$ = 114 N/mm² after corrosion exposure, while it remains unchanged for butt welds.
- The increase in fatigue strength for fillet welds is attributed to corrosion-induced smoothing of the initially sharp notch geometry.
- In contrast, corrosion slightly sharpens the initially mild notch of butt welds, resulting in a lower 50% quantile fatigue strength; however, this effect is not visible in the 95% quantile due to the higher scatter of uncorroded specimens.
- Clean blasting leads to a significant increase in fatigue strength, and this beneficial effect is not reduced by corrosion exposure.

These findings contribute to a more reliable assessment of the remaining fatigue life of existing offshore support structures and may support lifetime extension strategies.

ACKNOWLEDGEMENTS

The authors express their sincere gratitude for the financial support of the research project “Influence of corrosive media on the fatigue strength of offshore wind turbines (CorroFAT)”, grant number 37 LN/1, of the Research Association for Steel Applications (FOSTA) e. V. funded by the German Federal Ministry of Economics and Climate Action (BMWK) via the German Federation of Industrial Research Associations "Otto von Guericke" (AiF) e. V on the basis of a resolution of the German Bundestag.

REFERENCES

[1] Xu S, Qiu B. Experimental study on fatigue behavior of corroded steel. Materials Science and Engineering: A 2013;584:163–9. https://doi.org/10.1016/j.msea.2013.07.006.

[2] Xu S, Wang Y. Estimating the effects of corrosion pits on the fatigue life of steel plate based on the 3D profile.

Downloaded from asmedigitalcollection.asme.org/OMAE/proceedings-pdf/OMAE2026/89503/V003T03A008/7643707/v003t03a008-omae2026-182297.pdf by Deutsches Zentrum für Luft- und Raumfahrt (DLR) user on 02 October 2026

Copyright © 2026 by ASME; reuse license CC-BY 4.0

International Journal of Fatigue 2015;72:27–41. https://doi.org/10.1016/j.ijfatigue.2014.11.003.
[3] Shojai S, Kabha K, Woitzik C, Braun M, Ghafoori E. Fatigue behaviour of 12-month corroded offshore steel joints under accelerated salt spray exposure: an experimental and numerical analysis. Weld World 2025. https://doi.org/10.1007/s40194-025-02043-0.
[4] Shojai S, Schaumann P, Ghafoori E. Micro-support effect consideration in fatigue analysis of corroded steel based on real surface geometry. Journal of Constructional Steel Research 2024;212:108259. https://doi.org/10.1016/j.jcsr.2023.108259.
[5] Elahi SA, Sofiani FM. A numerical study on fatigue strength degradation of S355 structural steel due to pitting corrosion in the sea environment. Under review;2024.
[6] Mehri Sofiani F, Chaudhuri S, Elahi SA, Hectors K, Waele W de. Quantitative Analysis of the Correlation between Geometric Parameters of Pits and Stress Concentration Factors for a Plate Subject to Uniaxial Tensile Stress. Theoretical and Applied Fracture Mechanics 2023:104081. https://doi.org/10.1016/j.tafmec.2023.104081.
[7] Shojai S, Schaumann P, Braun M, Ehlers S. Influence of pitting corrosion on the fatigue strength of offshore steel structures based on 3D surface scans. International Journal of Fatigue 2022;164:107128. https://doi.org/10.1016/j.ijfatigue.2022.107128.
[8] Qvale P, Zarandi EP, Ås SK, Skallerud BH. Digital image correlation for continuous mapping of fatigue crack initiation sites on corroded surface from offshore mooring chain. International Journal of Fatigue 2021;151:106350. https://doi.org/10.1016/j.ijfatigue.2021.106350.
[9] Det Norske Veritas. Corrosion protection for wind turbines(DNV-GL RP-0416); 2016.
[10] International Standards Organization. ISO 8501-1:2007-12; Preparation of steel substrates before application of paints and related products - Visual assessment of surface cleanliness - Part 1: Rust grades and preparation grades of uncoated steel substrates and of steel substrates after overall removal of previous coatings (ISO 8501-1:2007).
[11] International Standards Organization. ISO 8503:2006: Surface roughness characteristics of blast-cleaned steel substrates; 2006.
[12] International Standards Organization. ISO 5817: Welding – Fusion-welded joints in steel, nickel, titanium and their alloys (beam welding excluded) – Quality levels for imperfections; 2014.
[13] ASTM International. Standard Practice for Preparation of Substitute Ocean Water (ASTM D1141); 1998.
[14] D19 Committee. Practice for the Preparation of Substitute Ocean Water. West Conshohocken, PA: ASTM International. https://doi.org/10.1520/D1141-98R21.
[15] DIN EN ISO 8407:2021-04, Korrosion von Metallen und Legierungen_- Entfernen von Korrosionsprodukten von Korrosionsprüfkörpern (ISO_8407:2021); Deutsche Fassung EN_ISO_8407:2021. Berlin: Beuth Verlag GmbH. https://doi.org/10.31030/3203640.
[16] Radaj D, Sonsino CM, Fricke W. Fatigue assessment of welded joints by local approaches. 2nd ed. Cambridge: Woodhead Publ. [u.a.]; 2006.
[17] Anthes RJ, Köttgen VB, SEEGER T. Kerbformzahlen von Stumpfstößen und Doppel-T-Stößen. Schweißen und Schneiden 1993(45 (12)):685–8.
[18] Renken F, Bock und Polach RUF von, Schubnell J, Jung M, Oswald M, Rother K et al. An algorithm for statistical evaluation of weld toe geometries using laser triangulation. International Journal of Fatigue 2021;149:106293. https://doi.org/10.1016/j.ijfatigue.2021.106293.
[19] Schubnell J, Jung M, Hieu Le C, Majid F, Braun M, Ehlers S et al. Influence of the optical measurement technique and evaluation approach on the determination of local weld geometry parameters for different weld types. Weld World 2020;64(2):301–16. https://doi.org/10.1007/s40194-019-00830-0.
[20] Dänekas C, Schubnell J, Krautheimer J, Jung M, Ghafoori E, Schaumann P. Algorithms for determination of weld toe radius and weld toe angle in welded joints. Journal of Constructional Steel Research 2025;224:109112. https://doi.org/10.1016/j.jcsr.2024.109112.
[21] European Committee for Standardization. Eurocode 3 - Design of steel structures - Part 1-9: Fatigue(EN 1993-1-9); 2020.
[22] Mehmanparast A, Brennan F, Tavares I. Fatigue crack growth rates for offshore wind monopile weldments in air and seawater: SLIC inter-laboratory test results. Materials & Design 2017;114:494–504. https://doi.org/10.1016/j.matdes.2016.10.070.

Downloaded from asmedigitalcollection.asme.org/OMAE/proceedings-pdf/OMAE2026/89503/V003T03A008/7643707/v003t03a008-omae2026-182297.pdf by Deutsches Zentrum für Luft- und Raumfahrt (DLR) user on 02 October 2026

Copyright © 2026 by ASME; reuse license CC-BY 4.0